Biomaterials 30 (2009) 4143–4151

Contents lists available at ScienceDirect

Biomaterials

journal homepage: www.elsevier.com/locate/biomaterials

Poly(vinyl alcohol)/poly(acrylic acid) hydrogel coatings for improving electrode–neural tissue interface

Yi Lu [a], Dingfang Wang [a], Tao Li [b], Xueqing Zhao [b], Yuliang Cao [a], Hanxi Yang [a], Yanwen Y. Duan [a,*]

[a] College of Chemistry and Molecular Sciences, Wuhan University, Wuhan, Hubei 430072, China
[b] Department of Neurology, Renmin Hospital, Wuhan University, Wuhan, Hubei 430060, China

ARTICLE INFO

Article history:
Received 12 February 2009
Accepted 21 April 2009
Available online 20 May 2009

Keywords:
Hydrogel coatings
Neural electrodes
Electrode–neural tissue interface
Neural prostheses
Tissue response
PVA/PAA IPNs

ABSTRACT

A major problem which hinders the applications of neural prostheses is the inconsistent performance caused by tissue responses during long-term implantation. The study investigated a new approach for improving the electrode–neural tissue interface. Hydrogel poly(vinyl alcohol)/poly(acrylic acid) interpenetrating polymer networks (PVA/PAA IPNs) were synthesized and tailored as coatings for poly(dimethylsiloxane) (PDMS) based neural electrodes with the aid of plasma pretreatment. Changes in the electrochemical impedance and maximum charge injection (Q_{inj}) limits of the coated iridium oxide microelectrodes were negligible. Protein adsorption on PDMS was reduced by ~85% after coating. In the presence of nerve growth factor (NGF), neurite extension of rat pheochromocytoma (PC12) cells was clearly greater on PVA/PAA IPN films than on PDMS substrates. Furthermore, the tissue responses of PDMS implants coated with PVA/PAA IPN films were studied by 6-week implantation in the cortex of rats, which found that the glial fibrillary acidic protein (GFAP) immunoreactivity in animals ($n = 8$) receiving coated implants was significantly lower ($p < 0.05$) compared to that of uncoated implants ($n = 7$) along the entire distance of 150 μm from the outer skirt to the implant interface. The coated film remained on the surface of the explanted implants, confirmed by scanning electron microscopy (SEM). All of these suggest the hydrogel coating is feasible and favorable to neural electrode applications.

1. Introduction

The rapid pace of recent advances in implantable miniature electronic devices has revealed great benefits for patients suffering from neural impairment and disorder, such as deafness, Parkinson's disease, epilepsy, blindness, intractable pain, and paralysis [1–7]. The neural prostheses and modulators recover damaged neurological function by selectively stimulating a small group of neurons in the peripheral or central nervous systems (CNS) through an electrode array [8–11]. Currently, one of the major problems that affect clinical applications of neural electrodes is the inconsistent performance caused by tissue responses after long-term implantation [12–16].

After implantation, an interaction will happen to some extent between the electrodes and proteins from the surrounding biological environment, which initiates biological inflammatory effect and subsequently leads to tissue encapsulation [17–20]. This increased the distance between electrode and target neurons and elevated the stimulation thresholds remarkably. Furthermore, the tissue encapsulation on the electrodes also hinders the diffusion of ions, thus causing a large increase in electrode impedance and thereby requiring higher compliant voltages to offset. It is obvious that tissue responses lead to not only an increase in the power consumption, but also the loss of neurons near the electrodes and in the end, a deterioration of functionality.

Many factors contribute to tissue response to implanted electrodes [12]. One is surgical trauma associated with electrode size, surface conditions, implanting procedures. Another is electrode materials and stimulation parameters. Some studies aimed to increase the charge injection (Q_{inj}) limits and bring down the electrode surface impedance (typically at 1 kHz), in order to reduce the electrode size [20–28]. Other works focused on the improvement of the substrate material–neural interface.

Actually, the exposure area of electrode substrate to tissue is considerably higher than the area of electrical conducting material exposed to tissue. Thus the chemical component and properties will have a dominant effect on tissue response over the conductor–tissue interface. Bioactive coatings for implantable electrodes have been extensively investigated for its potential to promote ingrowth of neural tissue and reduce sheer at the electrode–tissue

* Corresponding author. Tel.: +86 27 68752858; fax: +86 27 68753383.
E-mail address: yduan@whu.edu.cn (Y.Y. Duan).

0142-9612/$ – see front matter © 2009 Elsevier Ltd. All rights reserved.
doi:10.1016/j.biomaterials.2009.04.030

interface [14]. Winter and Cogan et al. used neurotrophin-eluting hydrogel as coatings for neural stimulating electrodes to promote their biocompatibility [20]. Klaver et al. decreased astrocyte proliferation by conjugation of transforming growth factor-beta one (TGF-beta 1) and laminin to dextran onto the substrate [29]. He et al. modified a silicon substrate with an anti-inflammatory peptide (alpha-MSH) to decrease the inflammatory responses [13]. Most of the research was carried out to improve silicon–tissue interface, which is relevant to the high density microelectrode array, made by microelectromechanical system (MEMS). In contrast, there were less works that were going on to advance the poly(dimethylsiloxane) (PDMS)–tissue interface, which is more closely associated with the applications of cochlear implant and deep brain stimulation [30–32].

Modifying the hydrophobic surface of PDMS with hydrogel films may reduce interface impedance and tissue response, which was suggested in our previous *in vivo* study of the impedance of cochlear implant electrodes chronically implanted in cats [30]. One of the reasons is possibly due to a decrease of non-specific protein adsorption and consequent tissue response on a hydrophilic surface [17–19]. Another reason is because hydrogel films provide a stable ionic conductive layer in contact with electrodes, resulting in reduction of electrode impedance [30]. It has also been reported that hydrogel coatings can promote nerve cell attachment and differentiation on electrode substrates [14]. Based on the merits of the non-degradative hydrogel films, including characteristics of drug release, high bulk ionic conductivity and low insertion friction of implantation, it is worth investigating other characteristics required by applications of neural electrodes. Among these, such as high Q_{inj}, low electrode impedance, less tissue response are important. The adhesion of a hydrogel film to PDMS and the swelling ratio of the film are all open to investigation.

One candidate hydrogel material is PVA/PAA interpenetrating polymer networks (PVA/PAA IPNs). PVA is a kind of poly hydroxyl polymer which is not degradable in most physiological situations [27]. PVA based hydrogels are broadly applied in tissue engineering, because of its excellent mechanical strength and good film-formation property [33–36]. PAA is a high water absorbing and protein resistive hydrogel material widely used in medical field [37–39].

In this study, we investigated the feasibility of tailoring PVA/PAA IPN hydrogel as coatings for implantable neural electrodes. The ionic conductivity of the tailored PVA/PAA IPNs was evaluated, and the electrode impedance and Q_{inj} of the electrodes coated with the film were investigated. Regarding the promotion of an improved electrode–neural tissue interface, the adsorption of protein and cell culture in the presence of the coating films was studied. Finally, the PDMS substrate coated with the PVA/PAA IPN hydrogel films was implanted into rats' cortex for 6 weeks, and the tissue response was assessed by analysis of glial fibrillary acidic protein (GFAP) immunoreactivity in the implant site.

2. Materials and methods

2.1. Synthesis of PVA/PAA IPNs

Aqueous PVA (M.W. 1,750, CP, Sinopharm, Shanghai, China) solution (2 wt%) was prepared by dissolving PVA in ultra-pure water (resistivity 18.25 MΩ/cm) at 90 °C under magnetic stirring. The solution was then cooled down to room temperature, and transferred into a three necked flask fitted with a condenser. An appropriate weight of acrylic acid (AA) monomer (CP, Sinopharm, Shanghai, China) was added into the PVA solution under magnetic stirring according to the desired ratios (0, 5, 10, 15 and 20 mol% of AA monomer per vinyl alcohol repeating unit). Ammonium persulfate (AR, Degussa-AJ, Shanghai, China) was added into the flask at 1000 ppm as an initiator. The mixed solution was purged with argon and stirred for 30 min, and then the flask was sealed and immersed in an oil bath at 80 °C. The reaction then took place for 48 h. The solution was filtered and kept overnight to remove the undissolved solids and bubbles, and the resulting homogeneous polymer solution was poured onto a PTFE plate to form a film for chemical characterizations. The excess water was evaporated slowly at 80 °C for 12 h in a vacuum oven. The reaction scheme is summarized in Fig. 1.

2.2. Sample preparations

Medical-grade platinum silicone elastomer (MDX4-4210, Factor II, US) was mixed thoroughly with its cross-linking catalyst and degassed under vacuum. For *in vitro* studies, PDMS films were made with a stainless steel mold and cured at 80 °C for 2 h. After curing, the samples were cooled down to room temperature before being removed from the mold and cut into small pieces (approximately 200 μm thick). For *in vivo* implantations, PDMS implants (1.0 mm in diameter and 5.0 mm in length with a round shape at the end) were made following the same method with another stainless steel mold.

The PDMS samples were ultrasonically cleaned with acetone and deionized water, then dried under vacuum for 12 h at 40 °C prior to use. Oxygen plasma treatment of the PDMS was carried out in a CTP-2000 k plasma generator (Corona Lab, Nanjing, China) for 1 min at a power of 100 W with an oxygen gas flow through the chamber. After this, the plasma treated samples were quickly immersed into a 2 wt% polymer solution for 30 min. Then the solution was removed and the coated PDMS samples were dried under vacuum for 12 h at 80 °C. All samples were sterilized by ethylene oxide gas prior to use.

2.3. Chemical characterization

2.3.1. FT-IR spectroscopy

Fourier transform infrared spectra (FT-IR) of prepared polymer films were performed with a Thermo Nicolet Avatar 360 FTIR Spectrometer. FT-IR spectra were measured on polymer films within the range of 4000–400 cm^{-1}.

2.3.2. Swelling experiments

Both the swelling ratio of polymer films in water and in bicarbonate/phosphate-buffered solution (CBS/PBS, pH ~ 7.4) [40] were evaluated. Dry polymer films were weighed and then immersed into the testing liquid for 48 h to reach swelling equilibrium at room temperature. Then the free liquid on the surface of the swollen films was removed quickly with filter paper, and the weights of the samples were measured again. The swelling ratio (SR) of the films is defined as follows:

$$SR = (m_t - m_o)/m_o \times 100\% \quad (1)$$

where m_o and m_t are the weight of dry and swollen films respectively.

2.3.3. Bulk ionic conductivity measurement

Both the bulk ionic conductivity of polymer films in water and in CBS/PBS were tested. Dry polymer films were cut into disks the same size as the test electrodes, and then immersed into testing liquid. After they were maintained at room temperature for 48 h, the free liquid on the surface of the films was removed. Then the polymer films were sandwiched between two symmetrical blocking stainless steel electrodes (each of ~1.77 cm^2 in geometrical area), and the AC impedance was measured in the frequency range between 100 kHz and 100 Hz with a 10-mV (rms) sinusoid signal by an impedance gain-phase analyzer (Solartron, 1260, UK). The bulk ionic conductivity (σ) of the films was determined from the following equation [41]:

$$\sigma = L/(S \times R) \quad (2)$$

where L, S, and R are the thickness, geometry area, and bulk resistance of the films respectively. The bulk resistance of the films was determined from the high-frequency intercept on the real impedance axis of the Cole–Cole plot.

2.3.4. Electrochemical measurement of coated AIROF electrodes

An iridium microelectrode was fabricated by sealing an iridium wire ($d = 100$ μm, 99.95%) into a glass capillary with a cross section diameter of approximately 3 mm. Activated iridium oxide films (AIROFs) microelectrodes were fabricated by activating iridium microelectrodes using the method in our previous works [23]. 4 μL of the polymer solution was pipetted onto each surface of the prepared AIROF microelectrodes and spread gently over the entire surface. The films were then dried at 80 °C for 4 h.

In all electrochemical experiments, electrodes were mounted in a three-electrode cell with a saturated calomel electrode (SCE) as reference electrode and a large-area platinum electrode as counter electrode. The working electrodes were immersed in testing solutions for at least 1 h to reach ionic equilibrium before the measurements.

Cyclic voltammetry (CV) measurements were made in 0.1 M phosphate buffered saline (PBS, pH 7.3) between potentials of −0.8 V and 0.6 V (vs. SCE) at a scan rate of 50 mV/s with a CH Instrument (CHI 634, Shenhua, China) at 25 °C. The cathodic charge storage capacity (CSC_C) of AIROF microelectrodes was calculated from the time integral of the cathodic current during one complete potential cycle [40]. The electrochemical impedance spectrum (EIS) of the test electrodes was measured in CBS/PBS at 25 °C with a potentiostat/galvanostat (Princeton Applied Research, 273A, US) and an impedance gain-phase analyzer (Solartron 1260, UK) using 10-mV (rms)

AC sinusoid signal at a frequency range from 100 kHz to 1 Hz at the open-circuit potential (vs. SCE). Zplot® and Zview® software (Scriber Associates Inc.) were used for the measurement and curve fitting analyses.

Safe charge injection (Q_{inj}) limits were determined experimentally by potential transient measurements. A symmetric charge balanced biphasic current pulse (shown in Fig. 7(A)), with 200 μs pulse width at 50 pulses per second (pps), was generated by a Neural Stimulator (Greentek, Wuhan, China) and applied to the AIROF microelectrode and a Pt counter electrode in CBS/PBS at 37 °C. The electrode potential excursion (shown in Fig. 7(B)) was recorded for the AIROF microelectrode against an SCE reference electrode with a digital oscilloscope (TPS202, Tektronix, China). The maximum Q_{inj} limits were obtained by continuously increasing the current amplitude of the pulses until the potential excursions reached either −0.6 V or 0.8 V (vs. SCE) after subtracting the voltage across the electrolyte (iR drop) (shown in Fig. 7(C)).

2.4. Protein adsorption

Fibrinogen (Calbiochem, CA) was labeled with ^{125}I using the iodogen method [19,42,43]. The labeled protein was dialyzed overnight against tris-buffered saline (TBS, pH 7.4) to remove radioactive free iodide. For studies of fibrinogen adsorption from buffer, labeled fibrinogen was mixed with unlabeled fibrinogen (labeled:unlabeled = 1:19) at a total concentration of 1 mg/mL. In all cases, surfaces of samples were equilibrated in TBS overnight prior to the adsorption experiments. PDMS, PVA coated PDMS, and PVA/PAA IPN hydrogel coated PDMS were incubated for 3 h in the radioactive protein solutions at room temperature, and then subsequently rinsed three times, 10 min each with TBS, wicked onto filter paper and transferred to clean tubes for radioactivity determination by gamma counting (1480 Perkin Elmer). Each type of sample was tested for three times, and radioactivity was converted to adsorbed protein amounts.

2.5. PC12 cell culture

As PC12 cells are well established as a model system to investigate neuronal differentiation when they are exposed to nerve growth factor (NGF) [44], they were used to study the neurite extensions on PVA/PAA IPN films. The seeds of PC12 cells were obtained from the American Type Culture Collection (ATCC) and cultured by the China Center for Type Culture Collection (CCTCC, Wuhan, China). All samples were coated with 0.1 mg/mL poly-L-lysine at 37 °C for at least 6 h, and rinsed with sterile water followed by 0.01 M PBS prior to use. PC12 cells were cultured in RPMI 1640 medium (Gibco, NY, US) supplemented with 10% fetalbovine serum (Gibco, NY, US), 5% horse serum (Gibco, NY, US), 2 mM L-glutamine (Gibco, NY, US), and 1% antibiotic/antimycotic (Sigma, South San Francisco, CA, USA). PVA/PAA IPN films and PDMS substrates were fixed on the bottom of a 24-well plate. PC12 cells were seeded at a density of 5×10^4 cells/mL to each well and followed by a 6-hour serum starvation [45]. 24 h after seeding, the cells were primed by adding 50 ng/mL nerve growth factor (NGF, Sigma, South San Francisco, CA, USA), and then maintained in a humidified incubator at 37 °C with 5% CO_2. The cultures were photographed with a Nikon Ti/S Inverted Microscope equipped with a DS-5MC-U2 digital camera on days 5 and 10.

2.6. Implantation study in vivo

2.6.1. Implantation procedures

Fifteen male adult Sprague–Dawley rats weighing 280–320 g were used for the chronic implantation experiment. The experimental protocol was approved by the Ethics Committee for Animal Research, Wuhan University, China. After anesthetized with 5% chloral hydrate (350 mg/kg), the rats were immobilized in a stereotaxic frame. A mid-saggital incision was made at the scalp and a 1.0 mm hole was created at 2 mm anterior to the bregma and 2 mm right lateral to midline with a portable rechargeable drill (QSCE, HITACHI, Japan). The implants (PDMS miniature bar, $d = 1.0$ mm, 5.0 mm length with a round tip at the end as control, $n = 7$, and PVA/PAA IPN hydrogel coated test sample, $n = 8$) were then very gently implanted into the cortex with the aid of an embedded fine needle. The overlying scalp was then sutured with 5–0 silk suture and the animals were monitored carefully until full recovery.

2.6.2. Tissue preparation and histological analysis

The rats were sacrificed for immunohistological analysis six weeks after the implantation ($n = 8$ for test group and $n = 7$ for control group). Rats were perfused transcardially with PBS followed by 4% paraformaldehyde in 0.1 M PBS, and the brains were removed and fixed in the same fixative at 4 °C for 48 h. Then the blocks around the implantation site were paraffin embedded and cut into a series of 6–8 horizontal sections (5 μm thick) per animal at the level of the hippocampus. Immunohistochemistry staining of GFAP was used to label astrocytes. Firstly, the

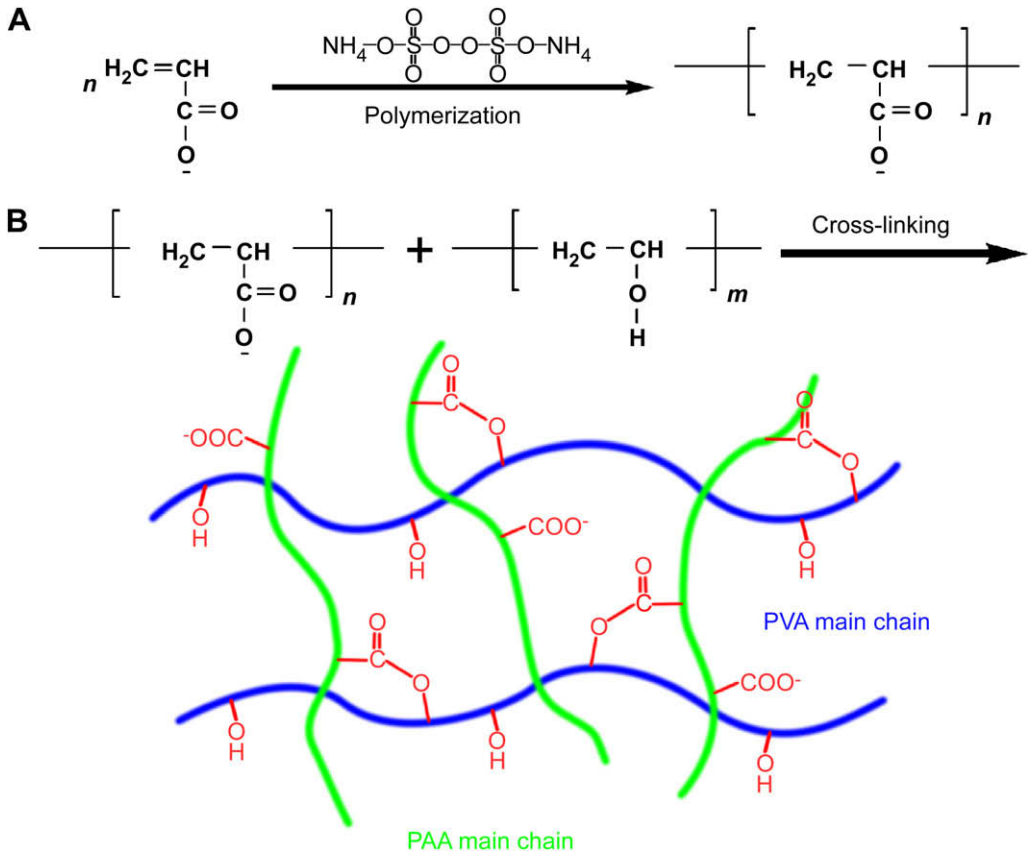

Fig. 1. (A) Scheme for polymerization of acrylic acid monomer; (B) Scheme for fabricating PVA with cross-linked PAA.

deparaffinized sections were boiled in 10 mM sodium citrate buffer (pH 6.0) for 20 min for antigen retrieval. The sections were then incubated with anti-GFAP antibody (1:500, polyclonal rabbit IgG, Dako) overnight at 4 °C. And then, appropriately matched secondary antibodies (Goat-Anti-Rabbit IgG, Boster, Wuhan, China) were applied for 20 min, followed by incubation with Streptavidin–Biotin-Complex for another 20 min at room temperature. The sections were incubated in diaminobenzidine (Boster, Wuhan, China) for visualization.

Digital images were collected using Olympus BX51 microscope equipped with a digital camera (Olympus) under 40× objective. All images were taken at the same conditions with the sample hole centered in the field of vision. The images were analyzed with Image-Pro Plus® 6.0 (Media Cybernetics; Silver Spring, MD) using a quantitative automated image analysis method. The intensity of GFAP was calculated as a function of distance up to the implant site.

Data were presented as mean ± standard error of the mean. Comparison of the implants at a discrete distance within 160 μm to the interface, with and without PVA/PAA IPN hydrogel coatings was evaluated with SPSS® 16.0 using Student's *t*-test analysis (two-tailed). Differences were considered significant at $p < 0.05$.

3. Results and discussion

3.1. FT-IR spectra

The FT-IR spectra of PVA/PAA IPN films with different PAA content (0, 5, 10, 15 and 20 mol% of AA monomer per vinyl alcohol repeating unit) are shown in Fig. 2. The FT-IR spectrum of pure PVA hydrogel membrane shows the main characteristic bands as follows: 3300 cm^{-1} at the O–H stretching vibration, 2941 cm^{-1} and 2910 cm^{-1} at the C–H stretching vibration, 1421 cm^{-1} and 1328 cm^{-1} at the C–H deformation vibration, 1241 cm^{-1} at the C–O stretching vibration, 1090 cm^{-1} at the C–O stretching vibration, and 917 cm^{-1} at the O–H bend.

With an increase of PAA content in hydrogels, the C=O stretching band of PAA at 1711 cm^{-1} was boosted up and shifted gently towards the lower wave numbers, while the C–O stretching vibration of pure PVA at 1241 cm^{-1} was gradually enhanced and broadened. This indicates that new intermolecular hydrogen bond interaction in the IPNs was formed, which is in evidence that hydrogen bond interactions of PVA hydrogel are replaced by hydrogen bond interactions between PVA and PAA [36]. Moreover, the peak of the O–H stretching vibration for the pure PVA membrane, at 3300 cm^{-1}, was gradually broadened and weakened, while the C–O stretching vibration at 1090 cm^{-1} was slightly strengthened. This may be caused by the esterification reaction between carboxylic acid groups in PAA and hydroxyl groups in PVA [46]. The study with the FT-IR spectra confirmed the formation of the PVA/PAA IPN hydrogel.

3.2. Swelling properties

The swelling results of different PVA/PAA IPN membranes in pure water and CBS/PBS are given in Fig. 3. As can be seen, the swelling ratio in pure water reaches a maximum in PVA/PAA IPN hydrogel with 5% PAA content. The carboxylic acid groups in PAA could form stronger hydrogen bonds with water than hydroxyl groups in PVA, thus the water uptake of PVA/PAA IPN hydrogel increased. However, further increase of the PAA content led to a decline of swelling ratio, because some of the carboxylic acid groups in PAA may have reacted with hydroxyl groups in PVA (shown in Fig. 1(B)) and also because the partly cross-linked PVA/PAA IPN hydrogel resulted in a more compact network and lesser swelling properties [46]. This result was in accordance with the FT-IR data, and it confirmed the partly cross-linked structure of PVA/PAA IPN hydrogels.

The water uptake of PVA/PAA IPN membranes in CBS/PBS (pH 7.4) was higher than in pure water, and it increased quickly with an increase in PAA content, because unreacted carboxylic acid groups in PVA/PAA IPN hydrogel reacted with the cations in CBS/PBS and the repulsion of carboxylic ions dissociated the intermolecular hydrogen bonding of the polymer [41]. Although the PVA/PAA IPN hydrogel with higher PAA content has a more compact network, as the PAA content increased, the amount of unreacted carboxylic acid groups also increased, and therefore the material tends to swell.

The swelling properties of the coating material are important for applications in neural electrodes, because it concerns the adhesion and stability of the coating film on the substrate, and a lesser tendency to swell would be a desirable criteria; on the other hand, the high water intake benefits the ionic mobility at the electrode interface, thus facilitating the electrical stimulation and recording of electrophysiological events.

3.3. Bulk ionic conductivity

The bulk ionic conductivity of different PVA/PAA IPN films in pure water and CBS/PBS is shown in Fig. 4. In pure water, the bulk ionic conduction of PVA/PAA IPN film is mainly caused by the transfer of H^+ ions of the carboxylic acid groups in the

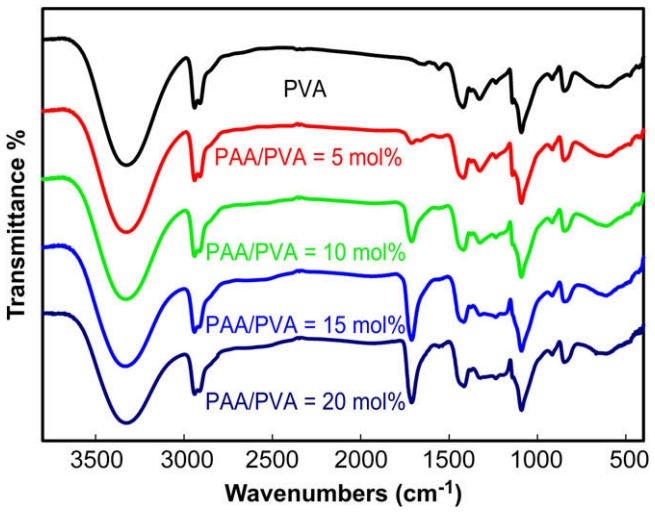

Fig. 2. FT-IR spectra of PVA/PAA IPNs (PAA/PVA = 0, 5, 10, 15 and 20 mol%, respectively.).

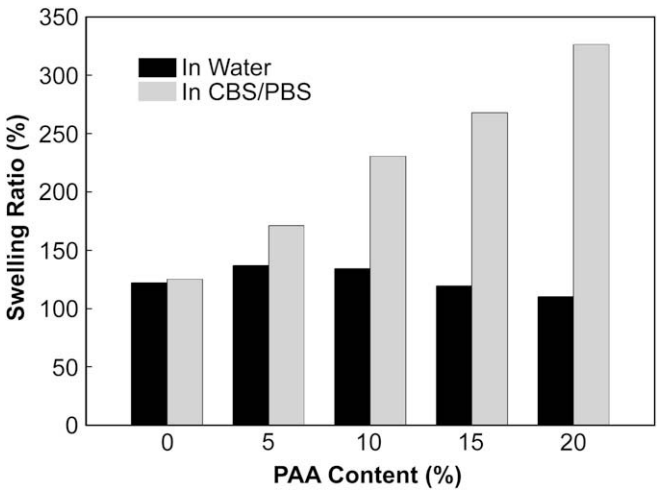

Fig. 3. Swollen ratios of PVA/PAA IPN membranes (PAA/PVA = 0, 5, 10, 15 and 20 mol%, respectively.) in water and CBS/PBS.

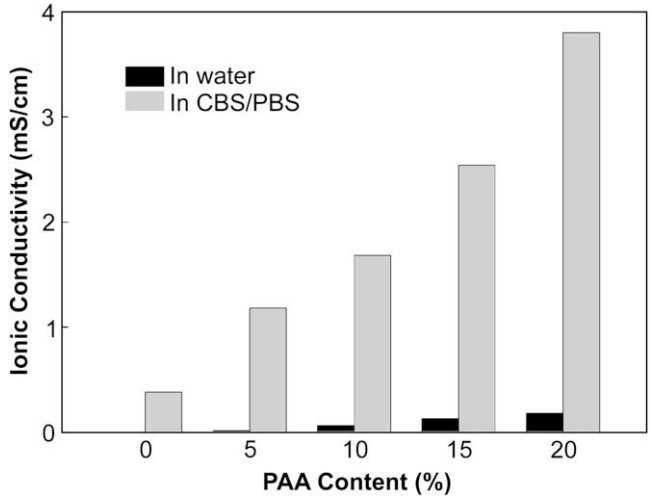

Fig. 4. Bulk ionic conductivities of PVA/PAA IPN membranes (PAA/PVA = 0, 5, 10, 15 and 20 mol%, respectively.) in water and CBS/PBS.

hydrogel membrane, which is proportional to the amount of unreacted carboxylic acid groups in the membrane. As the amount of free carboxylic acid groups in PVA/PAA IPN hydrogel increased with the increase of PAA content, the bulk ionic conductivity subsequently increased from 7×10^{-3} mS/cm to 1.8×10^{-1} mS/cm.

The bulk ionic conductivity in CBS/PBS was in the range of 0.1–10 mS/cm, and the ionic conduction takes place by a segmental motion mechanism [41,47] which can be explained as follows: a cation (typical Na^+ in CBS/PBS) is firstly associated with the oxygen atoms in a polymer chain, then the polymer chain gradually changes its conformation due to segmental motion so that the cation is transferred to the neighboring site. Because the increased proportions of PAA in the hydrogel increased the entropy as compared to the PVA hydrogel, so the segmental motion was subsequently increased, and the transfer of ions became easier. Also, as the water uptake of the PVA/PAA hydrogel increased, the amount of ions inside the membranes also increased, and this altogether resulted in an increase of bulk ionic conductivity in the PVA/PAA membranes.

It is clear that the PVA/PAA IPN hydrogels can be tailored by taking a different ratio of PAA in the synthesizing process to result in different levels of water absorption. An increase in water absorption on one hand causes large swelling and mechanical instability of the coatings on the substrate; on the other hand it enhances electrical signal transfer across the electrode interface by offering high ionic conductivity near the electrodes. Both aspects have to be considered and balanced in order to meet the requirements of neural electrodes, and the coating has to have low electrode impedance that remains stable through long-term implantation. Therefore, PVA/PAA IPN membranes with a PVA:PAA ratio of 10:1 was chosen as the best candidate coating material for further study.

3.4. Cyclic voltammograms

Iridium oxide is a biocompatible, corrosion resistant, and high charge storage capacity material, and these properties make it the ideal candidate material for electrical neural microstimulation [23,24]. An iridium oxide microelectrode was fabricated by applying electrical potential pulses to an iridium microelectrode in phosphate buffer solution, which is known as an AIROF microelectrode. In order to investigate the influence of hydrogel membrane coatings on electrode electrochemical behaviors, we evaluated the cyclic voltammograms, electrochemical impedance spectra, and charge injection limits of AIROF microelectrodes coated with PVA/PAA IPN films.

The cyclic voltammograms of AIROF microelectrodes before and after the electrodes were coated by PVA/PAA IPN films at a scanning rate of 50 mV/s in PBS are shown in Fig. 5. The cyclic voltammogram of AIROF electrodes exhibit distinct peaks correlated to the redox reactions of iridium oxides which are involved in the transfer of ions across the electrode–electrolyte interface. It can be seen that the PVA/PAA IPN film on the AIROF electrode provided a bridge to transfer ions. However, as the bulk ionic conductivity of PVA/PAA IPN hydrogel was lower compared to the ionic conductivity of PBS, so the ion transfer rate in the film was slower. When the ion transfer rate could not meet the reaction rate on the electrode–electrolyte interface, polarization was observed on the cyclic voltammogram, revealed as a reduction of the distinct peaks and a small position shift against the potential axis. Thus, the CSC_c of AIROF microelectrodes was decreased from $\sim$55 mC/cm^2 to $\sim$48 mC/cm^2, and the two oxidation peaks of iridium oxide at 0.2 V and 0.55 V were shifted to 0.3 V and 0.65 V respectively.

3.5. Electrochemical impedance spectra

An important factor to be addressed in neural prosthetic devices, especially for neural stimulation microelectrodes, is that the electrode material must be able to transfer charge under low interface impedance to minimize electrode polarization and power consumption. The impedance of a neural electrode at the frequency of 1 kHz is an important characteristic parameter, as it correlates to the power consumption during electrical neural stimulation as well as to noise in recording [21]. The EIS results of AIROF microelectrodes uncoated and coated with PVA/PAA IPN films at their open-circuit potentials in CBS/PBS, and a Randles type equivalent circuit are given in Fig. 6. After coating, the impedance of the microelectrodes at 1 kHz increased from 3.3 kΩ to 6.3 kΩ, still $\sim$84% lower than unactivated Ir microelectrodes (38.5 kΩ). It should be noted that the electrode impedance of chronic implanted cochlear electrodes can rise 2–4 times higher due to a reduction of free ions near the electrodes as a consequence of tissue response [30–32]. Thus

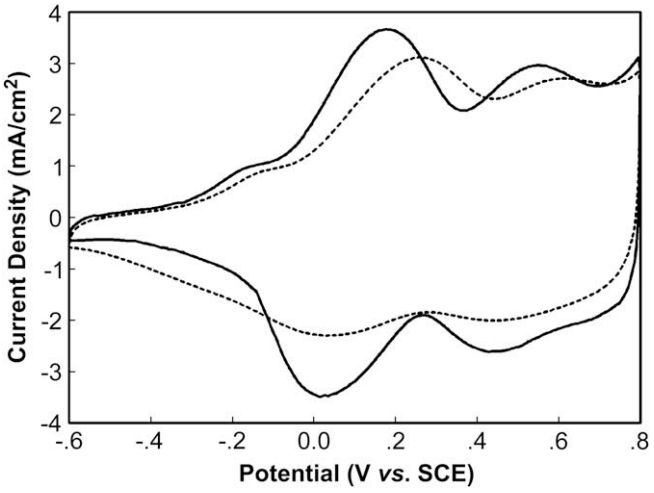

Fig. 5. Cyclic voltammograms of AIROF microelectrode (—) and PVA/PAA IPN (PAA/PVA = 10 mol%) films coated AIROF microelectrode (- - -) at a sweep rate of 50 mV/s in PBS.

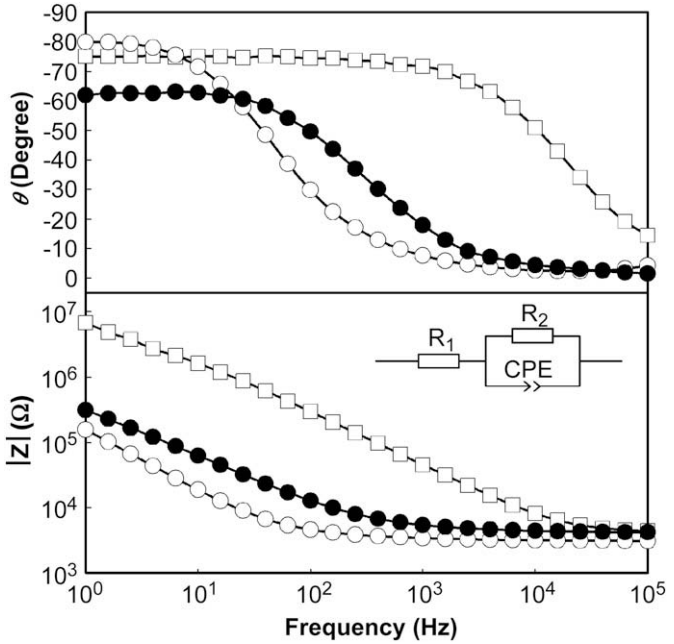

Fig. 6. Bode plot of electrochemical impedance of iridium microelectrode (□), AIROF microelectrode (○) and PVA/PAA IPN (PAA/PVA = 10 mol%) films coated AIROF microelectrode (●) in CBS/PBS.

the coated electrode should offer a good advantage in maintaining stable electrode impedance while it is dwelling in living tissue.

In EIS analysis, a constant phase element (CPE) was introduced, which represents a dispersive double layer capacitance and which reveals the non-homogeneity of the microelectrode surface and the microscopic distribution at the liquid–solid interface [30]. The concept of CPE is explained by the following equation:

$$Z(\mathrm{CPE}) = 1/\left[T(j\omega)^P\right] \quad (3)$$

where $j = \sqrt{-1}$, ω is the angular frequency (rads^{-1}) $= 2\pi f$, f is the frequency in Hz. The parameters of the CPE are defined by CPE-T and CPE-P. The parameter T indicates the value of the capacitance of the CPE, and it has the numerical value of $1/Z(\mathrm{CPE})$ at $\omega = 1$ rad/s. The parameter P reveals the micro fractal and distribution of the phase–phase interface. It can be affected by a series of factors, such as surface roughness, distribution of reaction rates, or a non-uniform current distribution. When $P = 1$, this CPE is identical to a capacitor, so Eq. (3) can be written as follows:

$$Z(\mathrm{CPE}) = 1/(Tj\omega) = 1/(Cj\omega) \quad (4)$$

Curve fitting of the results indicated that after coating with PVA/PAA IPN films, the value of CPE-T of the AIROF microelectrodes decreased from 1.26 $\mu\mathrm{F\,s}^{P-1}$ to 0.81 $\mu\mathrm{F\,s}^{P-1}$, compared to 0.02 $\mu\mathrm{F\,s}^{P-1}$ for the unactivated Ir microelectrodes. The value of CPE-P decreased from 0.92 to 0.73, which was similar to the unactivated Ir microelectrodes (0.75). This indicates that after activation, the pseudo-capacitance of the microelectrode increased sharply, and the AIROF microelectrode was closer to an ideal capacitance. However, after it was coated with PVA/PAA IPN films, the near electrolyte CBS/PBS was replaced by the PVA/PAA film with the lower ionic conductivity, leading to a slight decrease in the values of CPE-T and CPE-P. Considering the tissue response to chronically implanted electrodes, the electrolyte close by could dramatically change because of the presence of tissue encapsulation [30], and the presence of the PVA/PAA IPN hydrogel film can either provide a stable electrical contact to the surrounding tissue or reduce tissue response by its hydrophilic property and lesser insertion trauma. The advantages of PVA/PAA IPN hydrogel film coating could be pronounced under this circumstance.

3.6. Safe charge injection limits

The charge injection (Q_{inj}) limit is defined as the maximum quantity of charge per phase (pulse) and per electrode geometric area of a stimulus that an electrode can inject to PBS before reaching the water electrolysis potential. The Q_{inj} places a restriction on the minimum electrode size that can safely deliver a given stimulus or a maximum stimulus that can be safely delivered with a given electrode [23,24]. It is an important parameter determining the effect of electrical neural stimulation, and it correlates to the risk of electrode deterioration and tissue damage caused by electrical stimulation [23]. Fig. 7 shows the potential excursion on AIROF microelectrodes before and after coating with PVA/PAA IPN films at a charge injection density of 3.0 $\mathrm{mC/cm}^2$. The iR drop (access resistance) of the electrodes with the coating slightly increased, as the bulk ionic conductivity was lower than that of the electrode without the coating in CBS/PBS. After the iR drop was subtracted, the resulting curve represented the potential at the electrode surface, reflecting the charging/discharging of the pseudo-capacitor under the constant current pulse. However, as the low ion transfer rate controlled the reaction rate on the AIROF microelectrode, so the increased potential was due to the concentration polarization at the interface of the electrode–hydrogel.

The Q_{inj} of the AIROF microelectrodes with 0.2 ms anodic-first pulses at a frequency of 50 Hz was ~4.0 $\mathrm{mC/cm}^2$, while the value of Q_{inj} reduced to ~3.3 $\mathrm{mC/cm}^2$ for the electrodes coated with PVA/PAA IPN film. However, it was reported that the damage threshold for biological tissue is ~1 $\mathrm{mC/cm}^2$ [22], thus the decline of Q_{inj} value of AIROF microelectrodes after being coated with PVA/PAA IPN films can be neglected.

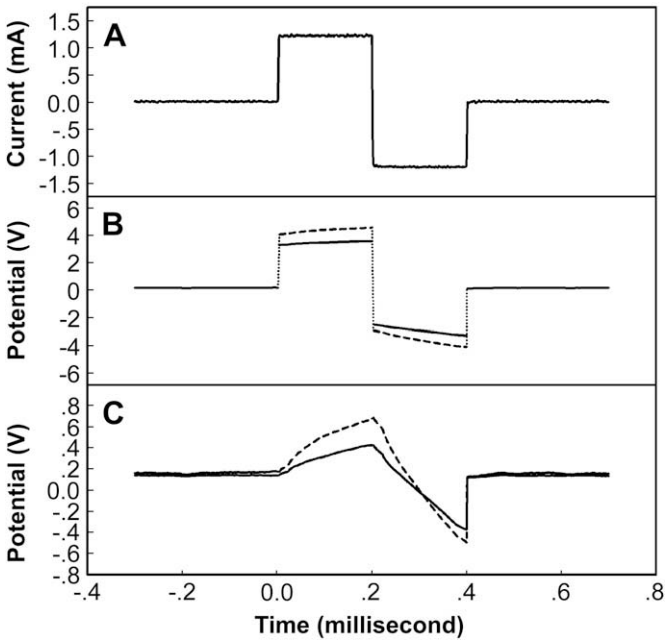

Fig. 7. Potential transient measurements of AIROF microelectrode (—) and PVA/PAA IPN (PAA/PVA = 10 mol%) films coated AIROF microelectrode (– – –) in CBS/PBS. (A) current pulse (charge injection density 3.0 $\mathrm{mC/cm}^2$) applied on the electrode; (B) potential transient of the electrode; (C) potential transient after subtracting iR drop (·····).

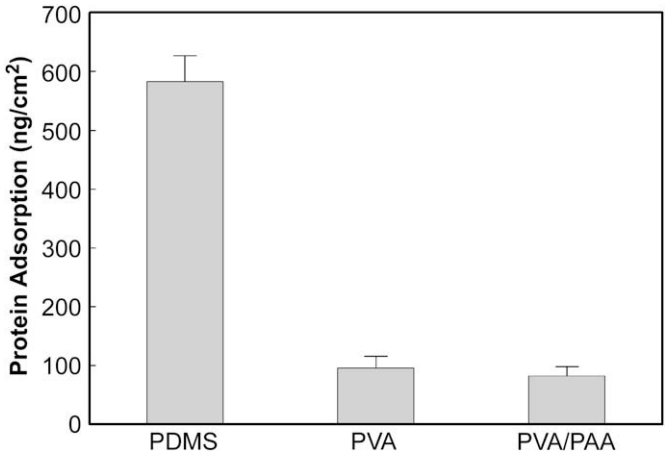

Fig. 8. Non-specific adsorption of protein (fibrinogen) on PDMS without coating, with PVA coatings, and with PVA/PAA IPN (PAA/PVA = 10 mol%) films coatings ($n = 3$).

3.7. Protein adsorption

It has been widely demonstrated that non-specific adsorption of a protein layer is responsible for mediating subsequent tissue response, and this is generally considered harmful to the performance of implants [42]. Fig. 8 shows protein adsorption to PDMS surfaces (control), PVA coated PDMS surfaces, and PVA/PAA IPN film (PAA/PVA = 10 mol%) coated PDMS surfaces, respectively. The non-specific adsorption of protein was approximately 586 ng/cm^2 on the PDMS surfaces, implying that a fibrinogen monolayer was formed on the unmodified surface [43]. However, fibrinogen adsorption decreased to 92 ng/cm^2 on PVA coated surfaces, and to 84 ng/cm^2 on PVA/PAA IPN coated surfaces. PAA is a common material for biosensors, and it exhibits good biocompatibility and protein resistance [48]. Moreover, PVA/PAA IPN coatings possess a much more ordered network than that of a PVA surface, so the protein adsorption was lowest on the PVA/PAA IPN coating.

3.8. PC12 cell culture

PC12 cells have been employed to study the effect of PVA/PAA IPN coatings on neurite extensions. We observed repeatedly that the cell densities on the coated surfaces were much higher than on the control surfaces. PC12 cells also exhibited neurite extension and neurite networks on the PVA/PAA IPN film at day 5 and day 10 after the cells were exposed to NGF. In contrast to the PVA/PAA IPN film, the cells on PDMS maintained an undifferentiated, rounded morphology with fewer extensions. This evidently demonstrated a much better cytocompatibility for neuronal phenotypes on PVA/PAA IPN than on PDMS.

3.9. GFAP immunostaining

When foreign materials such as electrodes are implanted into the host CNS, it elicits a tissue response that involves microglia,

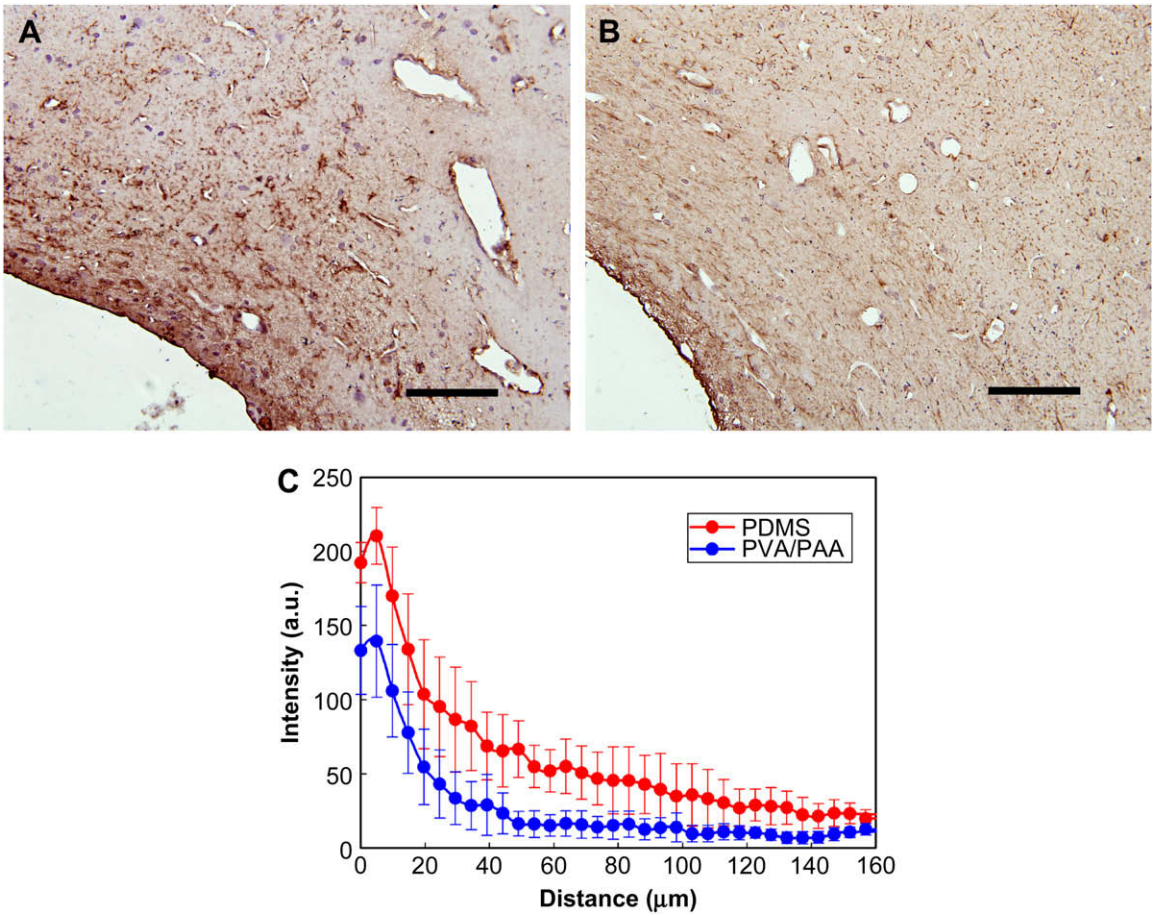

Fig. 9. GFAP immunostaining of uncoated (A) and PVA/PAA IPN (PAA/PVA = 10 mol%) films coated (B) PDMS implants after six weeks post-implantation (bar = 50 μm). Quantitative comparison of GFAP immunoreactivity between the uncoated and PVA/PAA IPN coated implants was made via GFAP intensity profiles as a function of distance from the insertion site (C).

macrophages, astrocytes, etc., which lead to the formation of a glial scar [12]. The astroglial encapsulation is a foreign body response to chronic implants, which is associated with a persistent inflammatory response consisting of activated microglia and a loss of neurons [15]. The encapsulation also results in elevated electrode impedance due to a reduction of available ions near electrodes [30]. As a consequence, the threshold of electrical stimulation may rise, and the stimulation protocol may possibly have to be adjusted to accommodate the changes of the electrode–neural tissue interface, which results in a decline of the efficacy of neural prostheses.

The tissue response is usually quantitatively assessed by the expression of GFAP, a maker of astrocyte [12,15,16]. In this study, two groups of implant samples (PDMS) with and without PVA/PAA IPN coating were implanted into the cortex of rats for 6 weeks. After the brain tissue of the experimental rats was prepared, the immunoreactivity of GFAP along the length from the outer skirt to implant interface was analyzed (Fig. 9). The results demonstrated that the intensity of GFAP immunostaining in the test group ($n = 8$) was significant lower ($p < 0.05$) than that of those in the control group ($n = 7$) along the entire length of 150 μm to the implant site. Fig. 9(A) and (B) are the microscopy photos of GFAP staining for the test and control groups, while Fig. 9(C) is a profile of the GFAP intensity at discrete distances up to 160 μm. The increased GFAP immunoreactivity was mainly located within 160 μm to the implant site, the finding agreeing with a previous study [12]. It found that GFAP immunoreactivity was within 500 μm from the implant at 1–4 weeks post-implantation, but as a more compact sheath formed after 6 weeks, the GFAP positive zone decreased to 50–100 μm around the insertion site [12].

The experimental results explicitly suggest that the PDMS electrode substrate coated with the PVA/PAA IPN film enables the reduction of the tissue response of CNS. The finding is consistent with the results of reduction of protein adsorption, as well as the promotion of neurite extension of PC12 cells found *in vitro*. It should be noted that the tissue response is not only greatly influenced by material properties, but also very much depends on the implanting trauma [12]. The reduction of tissue response found here could also be partially attributed to the low friction offered by the hydrogel coating which assists insertion and minimizes implantation trauma.

3.10. Stability of the coating

For chronically implantable electrodes, the coatings must be quite stable after long-term implantation. As PDMS is chemically inert and has low polarity [49], it is very difficult for it to be modified with other polymers. We attempted to apply plasma radiation on the PDMS implants under an oxygen flow, and in this way the entire surface of the PDMS implants was modified with active functional groups such as hydroxyl groups and carboxyl groups [50]. After the plasma treatment, the implants were immersed into the coating solution, and the hydrogel films were stabilized on PDMS implants via intramolecular hydrogen bonding between PVA/PAA IPN films and the active functional groups on the treated PDMS surfaces. The scanning electron microscopy study shows that no separation of the hydrogel film from the implant was observed, suggesting that the coating method is feasible and PVA/PAA IPN coatings are suitable for chronic implants.

4. Conclusion

This study has demonstrated the feasibility and advantages of synthesized PVA/PAA IPN hydrogel coating for improving the electrode–neural tissue interface. The tailored PVA/PAA IPN hydrogel exhibits good bulk ionic conductivity and proper swelling ratio in CBS/PBS. The hydrogel coated iridium oxide electrodes exhibit good electrochemical performance, and the changes in EIS, CV and Q_{inj} were negligible. The PVA/PAA IPN coatings reduced the protein adsorption by ~85% and also enhanced the neurite extension of PC12 cells. The GFAP immunoreactivity in animals ($n = 8$) receiving coated implants was significantly lower ($p < 0.05$) compared to that of uncoated implants ($n = 7$) along the entire distance of 150 μm from the outer skirt to the implant interface. Furthermore, PVA/PAA IPN coatings exhibit good stability and adhesion to plasma treated PDMS surfaces after 6 weeks of implantation, indicating that the coating method is practical and reliable. Finally, the study not only investigated the PVA/PAA IPN hydrogel, but more importantly it demonstrated a concept of neural electrode modification, in which hydrophilic properties are crucial.

Acknowledgement

The authors would like to thank Professor Hong Chen (Wuhan University of Technology) for her assistance in the protein adsorption measurement. The authors are grateful for the support by the National Nature Science Foundation of China (30570516) and the High Tech Research and Development (863) Program of China (2006AA02Z4E6).

References

[1] Frank MJ, Samanta J, Moustafa AA, Sherman SJ. Hold your horses: impulsivity, deep brain stimulation, and medication in parkinsonism. Science 2007;318(5854):1309–12.
[2] Rauschecker JP, Shannon RV. Sending sound to the brain. Science 2002;295(5557):1025–9.
[3] Hochberg LR, Serruya MD, Friehs GM, Mukand JA, Saleh M, Caplan AH, et al. Neuronal ensemble control of prosthetic devices by a human with tetraplegia. Nature 2006;442(7099):164–71.
[4] Makeig S, Westerfield M, Jung TP, Enghoff S, Townsend J, Courchesne E, et al. Dynamic brain sources of visual evoked responses. Science 2002; 295(5555):690–4.
[5] Sloviter RS. Decreased hippocampal inhibition and a selective loss of interneurons in experimental epilepsy. Science 1987;235(4784):73–6.
[6] Peyron R, Garcialarrea L, Deiber MP, Cinotti L, Convers P, Sindou M, et al. Electrical-stimulation of precentral cortical area in the treatment of central pain – electrophysiological and pet study. Pain 1995;62(3):275–86.
[7] North RB, Ewend MG, Lawton MT, Piantadosi S. Spinal-cord stimulation for chronic, intractable pain – superiority of multichannel devices. Pain 1991;44(2):119–30.
[8] Wadhwa R, Lagenaur CF, Cui XT. Electrochemically controlled release of dexamethasone from conducting polymer polypyrrole coated electrode. J Control Release 2006;110(3):531–41.
[9] Talwar SK, Xu SH, Hawley ES, Weiss SA, Moxon KA, Chapin JK. Behavioural neuroscience: rat navigation guided by remote control – free animals can be 'virtually' trained by microstimulating key areas of their brains. Nature 2002;417(6884):37–8.
[10] Jackson A, Mavoori J, Fetz EE. Long-term motor cortex plasticity induced by an electronic neural implant. Nature 2006;444(7115):56–60.
[11] Schiff ND, Giacino JT, Kalmar K, Victor JD, Baker K, Gerber M, et al. Behavioural improvements with thalamic stimulation after severe traumatic brain injury. Nature 2007;448(7153):600–U610.
[12] Polikov VS, Tresco PA, Reichert WM. Response of brain tissue to chronically implanted neural electrodes. J Neurosci Methods 2005;148(1):1–18.
[13] He W, McConnell GC, Schneider TM, Bellamkonda RV. A novel anti-inflammatory surface for neural electrodes. Adv Mater 2007;19(21):3529–33.
[14] Zhong YH, Yu XJ, Gilbert R, Bellamkonda RV. Stabilizing electrode-host interfaces: a tissue engineering approach. J Rehabil R D 2001 Nov–Dec;38(6): 627–32.
[15] Biran R, Martin DC, Tresco PA. Neuronal cell loss accompanies the brain tissue response to chronically implanted silicon microelectrode arrays. Exp Neurol 2005 Sep;195(1):115–26.
[16] He W, McConnell GC, Bellamkonda RV. Nanoscale laminin coating modulates cortical scarring response around implanted silicon microelectrode arrays. J Neural Eng 2006 Dec;3(4):316–26.
[17] Bridges AW, Singh N, Burns KL, Babensee JE, Andrew Lyon L, García AJ. Reduced acute inflammatory responses to microgel conformal coatings. Biomaterials 2008;29(35):4605–15.
[18] Van Beek M, Jones L, Sheardown H. Hyaluronic acid containing hydrogels for the reduction of protein adsorption. Biomaterials 2008;29(7):780–9.

[19] Chen H, Chen Y, Sheardown H, Brook MA. Immobilization of heparin on a silicone surface through a heterobifunctional PEG spacer. Biomaterials 2005;26(35):7418–24.
[20] Winter JO, Cogan SF, Rizzo JF. Neurotrophin-eluting hydrogel coatings for neural stimulating electrodes. J Biomed Mater Res B 2007;81B(2):551–63.
[21] Cogan SR. Neural stimulation and recording electrodes. Annu Rev Biomed Eng 2008;10:275–309.
[22] Wang K, Fishman HA, Dai HJ, Harris JS. Neural stimulation with a carbon nanotube microelectrode array. Nano Lett 2006 Sep;6(9):2043–8.
[23] Lu Y, Cai Z, Cao Y, Yang H, Duan YY. Activated iridium oxide films fabricated by asymmetric pulses for electrical neural microstimulation and recording. Electrochem Commun 2008;10(5):778–82.
[24] Lu Y, Wang T, Cai Z, Cao Y, Yang H, Duan YY. Anodically electrodeposited iridium oxide films microelectrodes for neural microstimulation and recording. Sens Actuat B 2009;137(1):334–9.
[25] Keefer EW, Botterman BR, Romero MI, Rossi AF, Gross GW. Carbon nanotube coating improves neuronal recordings. Nat Nanotechnol 2008 July;3(7):434–9.
[26] Green RA, Lovell NH, Wallace GG, Poole-Warren LA. Conducting polymers for neural interfaces: challenges in developing an effective long-term implant. Biomaterials 2008;29(24–25):3393–9.
[27] Lee KY, Mooney DJ. Hydrogels for tissue engineering. Chem Rev 2001;101(7):1869–79.
[28] Lee I-S, Whang C-N, Park J-C, Lee D-H, Seo W-S. Biocompatibility and charge injection property of iridium film formed by ion beam assisted deposition. Biomaterials 2003;24(13):2225–31.
[29] Klaver CL, Caplan MR. Bioactive surface for neural electrodes: decreasing astrocyte proliferation via transforming growth factor-beta 1. J Biomed Mater Res Part A 2007 Jun;81A(4):1011–6.
[30] Duan YY, Clark GM, Cowan RSC. A study of intra-cochlear electrodes and tissue interface by electrochemical impedance methods in vivo. Biomaterials 2004;25(17):3813–28.
[31] Xu J, Shepherd RK, Millard RE, Clark GM. Chronic electrical stimulation of the auditory nerve at high stimulus rates: a physiological and histopathological study. Hear Res 1997;105:1–29.
[32] Lim HH, Tong YC, Clark GM. Forward masking patterns produced by intracochlear electrical stimulation of one and two electrode pairs in the human cochlea. J Acoust Soc Am 1989;86(3):971–80.
[33] Teramura Y, Kaneda Y, Iwata H. Islet-encapsulation in ultra-thin layer-by-layer membranes of poly(vinyl alcohol) anchored to poly(ethylene glycol)–lipids in the cell membrane. Biomaterials 2007;28(32):4818–25.
[34] Mawad D, Martens PJ, Odell RA, Poole-Warren LA. The effect of redox polymerisation on degradation and cell responses to poly(vinyl alcohol) hydrogels. Biomaterials 2007;28(6):947–55.
[35] Choi J, Bodugoz-Senturk H, Kung HJ, Malhi AS, Muratoglu OK. Effects of solvent dehydration on creep resistance of poly(vinyl alcohol) hydrogel. Biomaterials 2007;28(5):772–80.
[36] Yue YM, Xu K, Liu XG, Chen Q, Sheng X, Wang PX. Preparation and characterization of interpenetration polymer network films based on poly(vinyl alcohol) and poly(acrylic acid) for drug delivery. J Appl Polym Sci 2008;108(6):3836–42.
[37] De Giglio E, Cometa S, Cioffi N, Torsi L, Sabbatini L. Analytical investigations of poly(acrylic acid) coatings electrodeposited on titanium-based implants: a versatile approach to biocompatibility enhancement. Anal Bioanal Chem 2007;389:2055–63.
[38] Dai JH, Bao ZY, Sun L, Hong SU, Baker GL, Bruening ML. High-capacity binding of proteins by poly(acrylic acid) brushes and their derivatives. Langmuir 2006;22(9):4274–81.
[39] Changez M, Koul V, Krishna B, Dinda AK, Choudhary V. Studies on biodegradation and release of gentamicin sulphate from interpenetrating network hydrogels based on poly(acrylic acid) and gelatin: in vitro and in vivo. Biomaterials 2004;25(1):139–46.
[40] Cogan SF, Guzelian AA, Agnew WF, Yuen TGH, McCreery DB. Over-pulsing degrades activated iridium oxide films used for intracortical neural stimulation. J Neurosci Methods 2004;137(2):141–50.
[41] Choudhury NA, Shukla AK, Sampath S, Pitchumani S. Cross-linked polymer hydrogel electrolytes for electrochemical capacitors. J Electrochem Soc 2006;153(3):A614–20.
[42] Chen H, Brook MA, Sheardown H. Silicone elastomers for reduced protein adsorption. Biomaterials 2004;25(12):2273–82.
[43] Chen H, Zhang Z, Chen Y, Brook MA, Sheardown H. Protein repellant silicone surfaces by covalent immobilization of poly(ethylene oxide). Biomaterials 2005;26(15):2391–9.
[44] Koh HS, Yong T, Chan CK, Ramakrishna S. Enhancement of neurite outgrowth using nano-structured scaffolds coupled with laminin. Biomaterials 2008;29(26):3574–82.
[45] Bergonzini V, Delbue S, Wang JY, Reiss K, Prisco M, Amini S, et al. HIV-Tat promotes cellular proliferation and inhibits NGF-induced differentiation through mechanisms involving Id1 regulation. Oncogene 2004;23(46):7701–11.
[46] Wang L, Li J, Lin Y, Chen C. Separation of dimethyl carbonate/methanol mixtures by pervaporation with poly(acrylic acid)/poly(vinyl alcohol) blend membranes. J Membr Sci 2007;305(1–2):238–46.
[47] Ratner MA, Shriver DF. Ion transport in solvent-free polymers. Chem Rev 1988;88(1):109–24.
[48] Wazawa T, Ishizuka-Katsura Y, Nishikawa S, Iwane AH, Aoyama S. Grafting of poly(ethylene glycol) onto poly(acrylic acid)-coated glass for a protein-resistant surface. Anal Chem 2006;78(8):2549–56.
[49] Intra J, Glasgow JM, Mai HQ, Salem AK. Pulsatile release of biomolecules from polydimethylsiloxane (PDMS) chips with hydrolytically degradable seals. J Control Release 2008;127(3):280–7.
[50] Chu PK, Chen JY, Wang LP, Huang N. Plasma-surface modification of biomaterials. Mat Sci Eng R 2002 Mar;36(5–6):143–206.